

# 1 A model-based approach to improve intranasal sprays 2 for respiratory viral infections

3 Saikat Basu<sup>1,\*</sup>, Mohammad Mehedi Hasan Akash<sup>1</sup>, Yueying Lao<sup>2</sup>, Pallavi  
4 A Balivada<sup>2</sup>, Phoebe Ato<sup>2</sup>, Nogaye K Ka<sup>2</sup>, Austin Mituniewicz<sup>3</sup>, Zachary  
5 Silfen<sup>2</sup>, Julie Suman<sup>4</sup>, Arijit Chakravarty<sup>5</sup>, Diane Joseph-McCarthy<sup>2,6</sup>

6 <sup>1</sup> Department of Mechanical Engineering, South Dakota State University, Brookings,  
7 SD 57007, United States

8 <sup>2</sup> Department of Biomedical Engineering, Boston University, MA 02215, United  
9 States

10 <sup>3</sup> Joint Department of Biomedical Engineering, University of North Carolina – North  
11 Carolina State University, Chapel Hill, NC 27599, United States

12 <sup>4</sup> Next Breath – an Aptar Pharma Company, Baltimore, MD 21227, United States

13 <sup>5</sup> Fractal Therapeutics, Cambridge, MA 02319, United States

14 <sup>6</sup> Bioengineering Technology and Entrepreneurship Center, Boston University, MA  
15 02215, United States

16 E-mail: \* Saikat.Basu@sdsstate.edu

17 **Abstract.** Drug delivery for viral respiratory infections, such as SARS-CoV-2, can  
18 be enhanced significantly by targeting the nasopharynx, which is the dominant initial  
19 infection site in the upper airway, for example by nasal sprays. However, under the  
20 standard recommended spray usage protocol (“Current Use”, or CU), the nozzle enters  
21 the nose almost vertically, resulting in sub-optimal deposition of drug droplets at the  
22 nasopharynx. Using computational fluid dynamics simulations in two anatomic nasal  
23 geometries, along with experimental validation of the generic findings in a different  
24 third subject, we have identified a new “Improved Use” (or, IU) spray protocol. It  
25 entails pointing the spray bottle at a shallower angle (almost horizontally), aiming  
26 slightly toward the cheeks. We have simulated the performance of this protocol for  
27 conically injected spray droplet sizes of 1 – 24  $\mu\text{m}$ , at two breathing rates: 15 and  
28 30 L/min. The lower flowrate corresponds to resting breathing and follows a viscous-  
29 laminar model; the higher rate, standing in for moderate breathing conditions, is  
30 turbulent and is tracked via Large Eddy Simulation. The results show that (a) droplets  
31 sized between  $\sim 6 - 14 \mu\text{m}$  are most efficient at direct landing over the nasopharyngeal  
32 viral infection hot-spot; and (b) targeted drug delivery via IU outperforms CU by  
33 approximately 2 orders-of-magnitude, under the two tested inhalation conditions. Also  
34 quite importantly, the improved delivery strategy, facilitated by the IU protocol, is  
35 found to be robust to small perturbations in spray direction, underlining the practical  
36 utility of this simple change in nasal spray administration protocol.

37 (249 words)

38 *Keywords:* Intranasal drug delivery; Respiratory transport; Nasal sprays; COVID-19;

39 Upper airway infection

**NOTE: This preprint reports new research that has not been certified by peer review and should not be used to guide clinical practice.**

## 40 1. Introduction

41 The global respiratory pandemic<sup>1</sup> caused by the severe acute respiratory syndrome  
42 coronavirus 2 (SARS-CoV-2) has thrust the field of fluid mechanics back into public  
43 eye, perhaps for the first time since the era of 1960s' space race.<sup>2</sup> Flow physics plays an  
44 essential role in almost every aspect of respiratory viral infections; none the more so than  
45 in targeted delivery of drugs to the infection hot-spots along the airway. Upper airway  
46 sites, in specific the ciliated epithelial cells that line the back of the nasal cavity at the  
47 nasopharynx (see Fig. 1) and are rich in angiotensin-converting enzyme 2 (ACE2) surface  
48 receptors, have been marked out<sup>3-5</sup> as the trigger zones for infection onset owing to  
49 SARS-like airborne viral respiratory pathogens. An early intervention method that can  
50 target the initial dominant infection site, i.e. the nasopharynx, is hence imperative for  
51 limiting asymptomatic transmission of the exhaled pathogenic particulates as well as for  
52 preventing systemic lower airway progression of the disease in a host, aggravating toward  
53 severe illness.<sup>6,7</sup> Of critical interest here, based on the brisk pace at which lower airway  
54 infections ensue after the emergence of initial symptoms, it has been conjectured<sup>3,8,9</sup>  
55 that the nasopharynx also acts as the seeding zone for spread of the disease to the lungs  
56 via lower airway aspiration of virus-laden boluses of nasopharyngeal fluids. Another

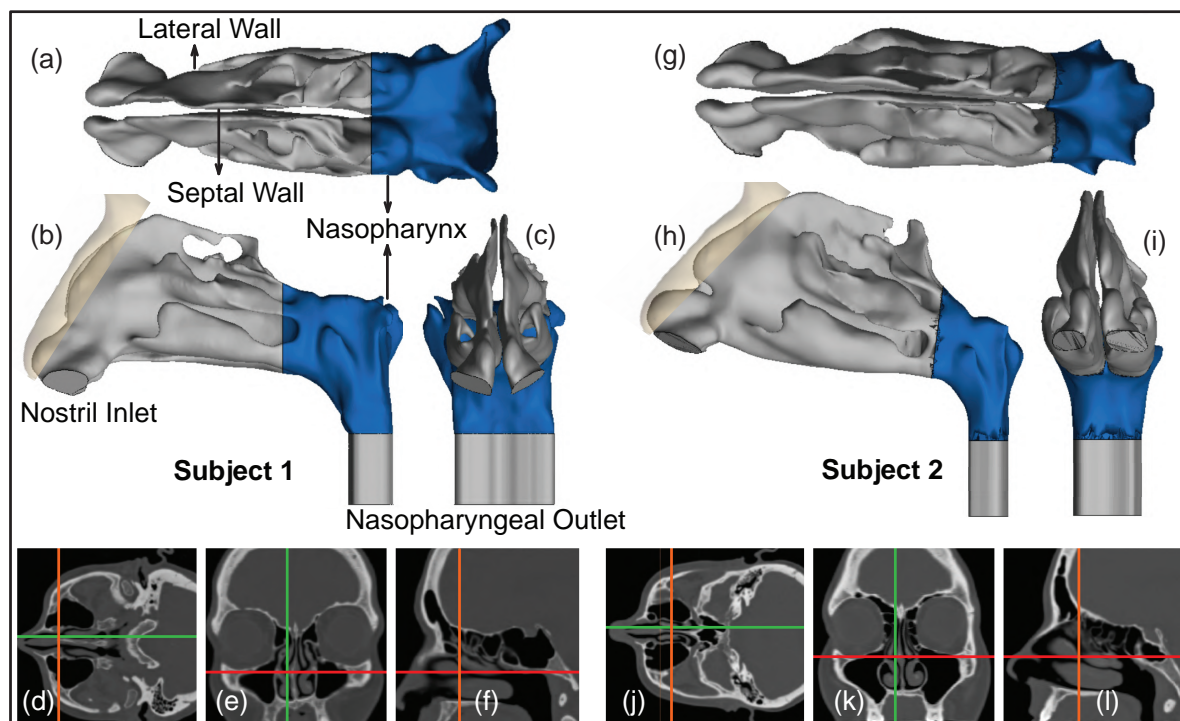


**Figure 1:** Panels (a) – (c) respectively show the axial, sagittal, and coronal views of the computed tomography (CT) based upper airway reconstruction in Subject 1. Panels (d) – (f) depict representative CT slices for the same subject. Therein, the green lines in (d) and (e) correspond to the location of the sagittal section shown in (f); the orange lines in (d) and (f) correspond to the location of the coronal section shown in (e); the red lines in (e) and (f) correspond to the location of the axial section shown in (d). Panels (g) – (i) respectively show the axial, sagittal, and coronal views of the CT-based upper airway reconstruction in Subject 2. Panels (j) – (l) depict representative CT slices for the same subject. Therein, the green lines in (j) and (k) correspond to the location of the sagittal section shown in (l); the orange lines in (j) and (l) correspond to the location of the coronal section shown in (k); the red lines in (k) and (l) correspond to the location of the axial section shown in (j). The nasopharynx has been marked in blue in panels (a) – (c) and (g) – (i).

57 concern is the mutation rate of SARS-CoV-2 and how the nature of the fitness landscape  
58 renders the virus amenable to evolving, potentially resulting in more virulent strains.<sup>10</sup>  
59 A nasal spray – that can administer nasal hygiene products, prophylactics, and antiviral  
60 agents – would address these concerns if it can efficiently deliver the pharmaceuticals at  
61 the virus-affected upper airway sites, thereby reducing the risk of viral droplet/aerosol  
62 shedding as well as mutation within the host.

63 While the nasal sprays do provide a simple, yet robust, drug delivery modality,  
64 especially during the infection onset phase of respiratory viruses; the choice still comes  
65 with at least two key open questions, *viz.* (a) what are the intranasally sprayed drug  
66 droplet sizes that would maximize targeted delivery at the initial dominant infection  
67 site, the nasopharynx?; and (b) is there a way to revise the nasal spray usage protocols,  
68 to enhance the delivery of drugs at the infected site?

69 This study addresses the above questions through implementing experimentally-  
70 validated computational fluid dynamics (CFD) modeling of the respiratory transport  
71 process in computed tomography (CT)-based anatomically realistic upper airway  
72 geometries. The related simulations replicate sprayed drug transmission against two  
73 different ambient inhalation rates, *viz.* 15 and 30 L/min; standing in respectively for  
74 relaxed and moderate steady breathing conditions.<sup>11</sup> Preliminary findings pertaining  
75 to this work have been presented at the American Physical Society’s Division of Fluid  
76 Dynamics Annual Meeting 2021.<sup>12</sup>

## 77 2. Materials and methods

### 78 2.1. Anatomic upper airway reconstruction

79 The *in silico* upper airway geometries used here were reconstructed from the de-identified  
80 medical-grade CT imaging data derived from two healthy test subjects. Subject 1 was  
81 a Caucasian female in the age range 61-65 years; Subject 2 was a Caucasian female  
82 in the age range 36-40 years. Use of the archived and anonymized medical records was  
83 approved with exempt status by the Institutional Review Board (IRB) for the University  
84 of North Carolina (UNC) at Chapel Hill, with informed consent waived for retrospective  
85 use in computational research.

86 In terms of imaging resolution, the  
87 CT slices of the airway cavities were ex-  
88 tracted at coronal depth increments of  
89 0.348 mm in Subject 1’s scans and 0.391  
90 mm in Subject 2’s scans. Digitization of  
91 the anatomic airspaces was carried out  
92 on the image processing software Mimics  
93 Research v18.0 (Materialise, Plymouth,  
94 Michigan), using a radio-density delin-  
95 eation range of -1024 to -300 Hounsfield

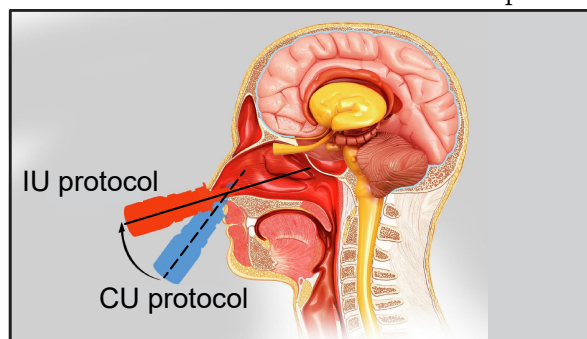


**Figure 2:** The schematic shows the two tested nasal spray usage protocols, *viz.* “Current Use” (or CU, represented by the dashed line) and “Improved Use” (or IU, represented by the solid line). Cartoon illustration is by the Dr. Ferrer Biopharma (Hallandale Beach, FL) graphics design team.

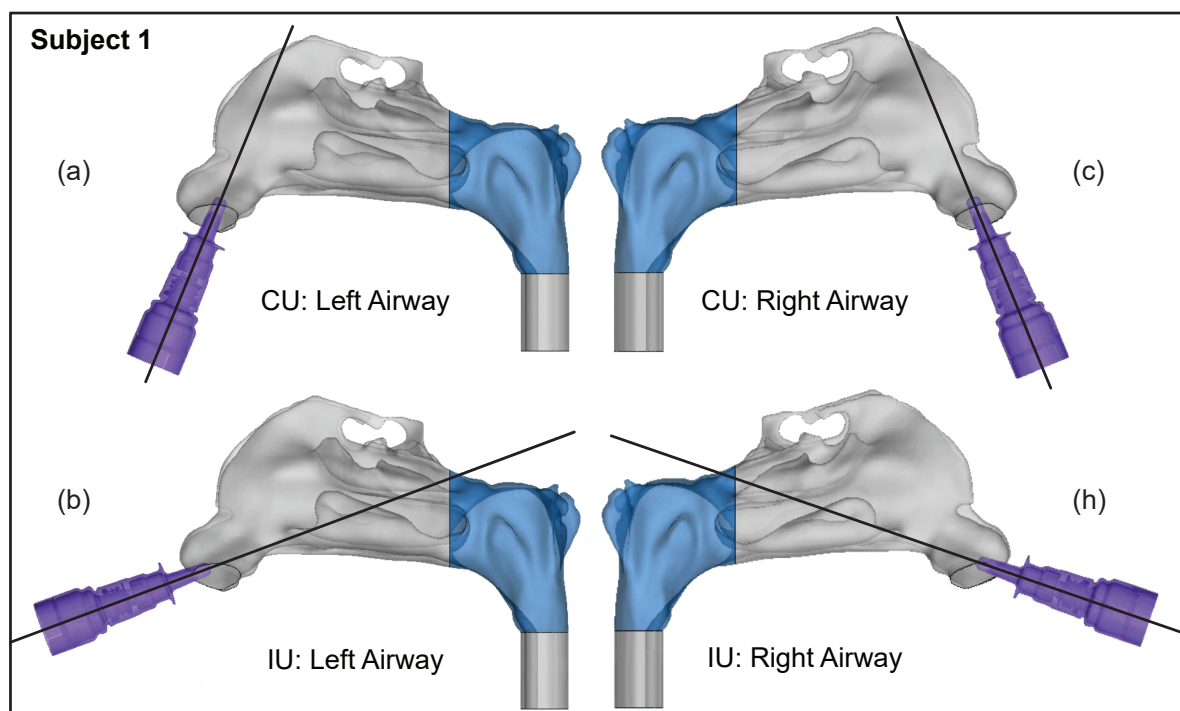


**Figure 3:** Spatial differences between the Current Use (CU) and Improved Use (IU) spray placement protocols, as visible sagittally in Subject 1. Nasopharynx is marked in blue.

96 units, and was complemented by clinically-monitored hand-editing of the selected pix-  
97 els to ensure anatomic accuracy. The output STL (stereolithography) geometries were  
98 then spatially meshed on ICEM-CFD 2019 R3 (ANSYS Inc., Canonsburg, Pennsyl-  
99 vania) with minute volume elements. Therein to confirm grid-independent solutions,  
100 established mesh-refinement protocols<sup>13,14</sup> were followed such that each computational  
101 grid contained more than 4 million unstructured, graded, tetrahedral elements. To en-  
102 able accurate tracking near tissue surfaces, further mesh refinement involved adding  
103 three prism layers at the cavity walls, with 0.1-mm thickness and a height ratio of 1.

## 104 2.2. Simulation of breathing transport and drug delivery

105 Inhalation parameters for gentle-to-moderate breathing conditions were numerically  
106 replicated at 15 and 30 L/min.<sup>11</sup> The lower flow rate commensurate with resting  
107 breathing is dominated by viscous-laminar steady-state flow physics.<sup>15-20</sup> The higher  
108 flow rates however trigger shear-induced<sup>21-23</sup> flow separation from the tortuous cavity  
109 walls, resulting in turbulence,<sup>24-27</sup> which was tracked through Large Eddy Simulation  
110 (LES), with sub-grid scale Kinetic Energy Transport Model<sup>28</sup> accounting for the  
111 small-scale fluctuations. The computational scheme on ANSYS Fluent 2019 R3  
112 employed a segregated solver, with SIMPLEC pressure-velocity coupling and second-  
113 order upwind spatial discretization. Solution convergence was monitored by minimizing  
114 mass continuity and velocity component residuals, and through stabilizing mass flow  
115 rate and static pressure at airflow outlets (see the nasopharyngeal outlet location in  
116 Fig. 1). For the pressure gradient-driven laminar airflow solutions, the typical execution



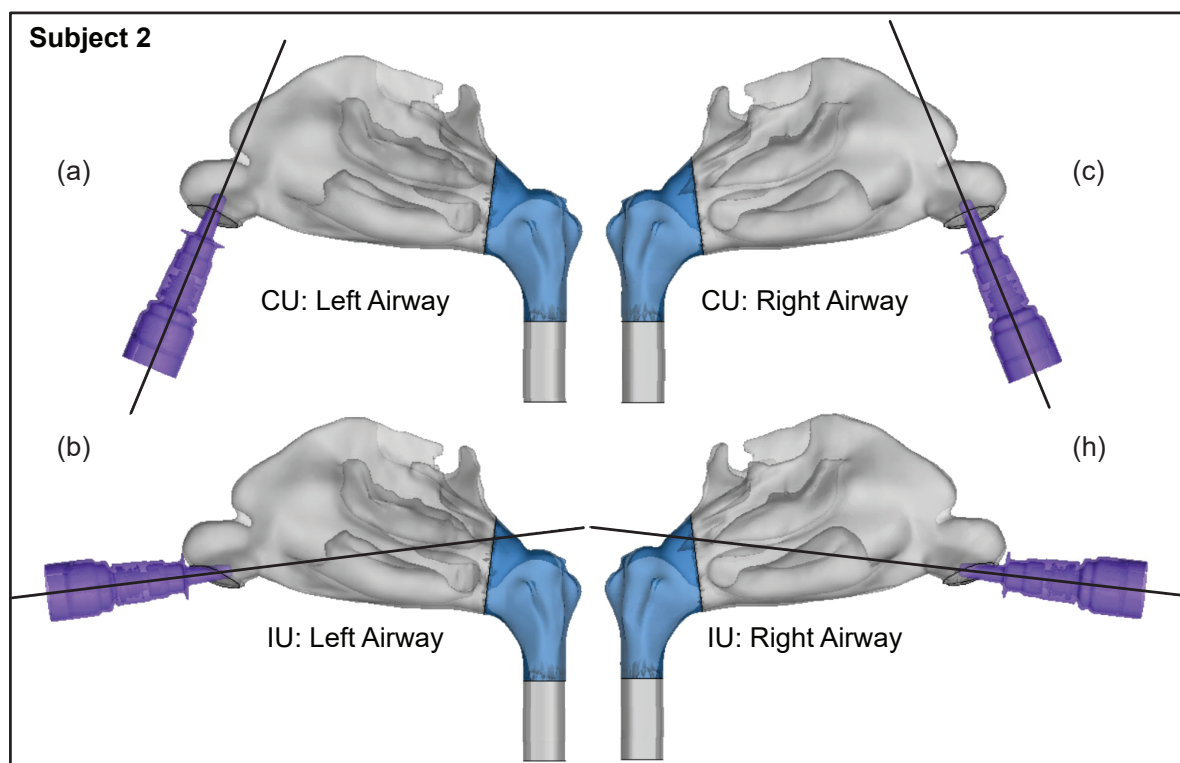


**Figure 4:** Spatial differences between the Current Use (CU) and Improved Use (IU) spray placement protocols, as visible sagittally in Subject 2. Nasopharynx is marked in blue.

117 time for 5000 iterations was 2–3 hours with 4-processor based parallel computations  
118 operating at 3.1 GHz speed on Xeon nodes. Additionally, the LES computations each  
119 required a run-time of 1–2 days, for a pressure-driven simulated flow interval of 0.25  
120 s, with a time-step of 0.0001 s. To realistically capture the inhaled warmed-up air  
121 transport along the respiratory pathway, its density and dynamic viscosity were set at  
122  $1.204 \text{ kg/m}^3$  and  $1.825 \times 10^{-5} \text{ kg/m.s}$ , respectively.

123 Spray dynamics against the ambient airflow was tracked via Lagrangian-based  
124 inert discrete phase simulations with a Runge-Kutta solver, with localized droplet  
125 clustering along intranasal tissues obtained through numerically integrating the  
126 transport equations that consider airflow drag, gravity, and other body forces relevant  
127 for small particulates, e.g., the Saffman lift force, and by implementing a no-slip trap  
128 boundary condition on the cavity walls. Note that Brownian effects were neglected in  
129 view of the tracked droplet sizes. The drug formulation density was set to 1.5 g/ml. All  
130 simulations released monodispersed inert drug droplets ranging in diameters from 1 – 24  
131  $\mu\text{m}$ , with 3000 monodispersed inert droplets being released during each iteration. The  
132 droplets were injected into the airspace from a single source point where the spray nozzle  
133 is located, streaming out in a hollow-cone shape, mimicking the action of a nasal spray;  
134 this method of release is referred to as a cone injection. The Valois VP7, an affordable  
135 mass-produced pharmaceutical nasal spray pump, with its accompanying dimension  
136 properties, such as plume angle and initial spray velocity, was used as an initial point  
137 of reference for the cone injections.<sup>29</sup> The droplets were given an initial velocity of 10

138 m/s<sup>30</sup> and a total flow rate of  $1 \times 10^{-20}$  kg/s. The plume angle and insertion depth  
139 were selected<sup>15</sup> to be 27.93° and 5 mm, respectively; by varying the spray direction  
140 – an optimal usage condition that augments droplet deposition at the target site was  
141 identified. See our earlier publications<sup>5,15</sup> for additional details on the numerical setup.

### 142 *2.3. On how to hold the spray bottle*

143 A key parameter for targeted delivery is the direction of the nasal spray axis, as  
144 the sprayed droplet trajectories are often inertia-dominated.<sup>15,18,31,32</sup> Instructional  
145 ambiguities<sup>33,34</sup> point toward a lack of definitive knowledge on the best ways to  
146 use a nasal spray device, with different commercial sprayers often offering somewhat  
147 contrasting recommendations. There is, however, a consensus that the patient should  
148 tilt her/his head slightly forward, while holding the spray bottle upright.<sup>33,35</sup> There  
149 is an additional clinical recommendation to avoid pointing the spray directly at the  
150 septum, which is the separating cartilaginous wall between the two sides of the nasal  
151 cavity. These suggestions were adopted in our standardization<sup>15,36</sup> of “Current Use”  
152 (CU) protocol for topical sprays. The digital models were inclined forward by an angle  
153 of 22.5°, and the vertically-placed upright<sup>33</sup> spray axis was aligned closer to the lateral  
154 nasal wall, at one-third of the distance between the lateral side and septal wall. Finally,  
155 the spray bottle was placed at the nostril to penetrate 5-mm into the airspace, to conform  
156 with the package recommendations of commercial sprayers<sup>35</sup> for a “shallow” intranasal  
157 nozzle placement.

158 While the CU protocol would provide the acceptable state-of-art for targeted drug  
159 delivery with nasal sprayers, the key focus of this study was to perturb that spray  
160 direction to test alternate protocols that bear the promise to improve delivery of drugs  
161 at the nasopharyngeal infection site. Our earlier findings<sup>15</sup> showed that to target the  
162 clinical site of ostiomeatal complex, or OMC (a key target site for corticosteroid-based  
163 topical therapeutic management for chronic rhinosinusitis<sup>15,19</sup> and allergic rhinitis<sup>37</sup>),  
164 the spray axis should be oriented to pass through the OMC itself. The inertial motion of  
165 the sprayed particulates assists such transport mechanism. Taking cue, to optimize the  
166 spray administration protocol in the current study, we oriented the nozzle such that the  
167 spray axis passes through the nasopharynx, and have named the strategy as “Improved  
168 Use”, or IU protocol. When determining the IU direction, it was important to satisfy  
169 three conditions as a way of ensuring the optimal placement of a nasal spray for drug  
170 release: (i) the extended spray axis for the IU protocol must intersect the nasopharynx;  
171 (ii) the spray axis must not cut through the septal wall; and (iii) the axis should intersect  
172 the lateral wall in the posterior part of the nasal cavity. See the cartoonized Fig. 2 for  
173 a broad-spectrum visual difference between the presently recommended CU and the  
174 to-be-tested IU protocols. Additionally, Figs. 3 and 4 depict the spatial distinctions in  
175 spray placement between the IU and CU protocols, in the two test subjects, as visible  
176 from the sagittal perspective.

177 2.4. Tolerance sensitivity analysis

178 Once the IU for an airway reconstruction was determined (following guidelines described  
179 in Section 2.3), a tolerance sensitivity study was performed to assess how far the user  
180 could deviate from the determined IU spray direction and still get similar regional drug  
181 deposition results, or in other words how robust (or, on the contrary, user-sensitive) the  
182 chosen IU direction really is.

183 To generate the new perturbed axes in the *in silico* space, a 1-mm radius circle  
184 was created perpendicular to the perturbed direction either 5-mm or 10-mm away from  
185 the central point on the nostril plane of each model. The two different distances were  
186 chosen in order to test the sensitivity of the results to different perturbation trends.  
187 The 5-mm method was performed on the left nostril of the subjects, while the 10-  
188 mm method was performed on the right nostril. Five peripheral points equidistant  
189 from each other were then selected on the circle created. The axis formed between the  
190 centroid point on the nostril plane and the peripheral point on the circle determined  
191 the new perturbed direction. In all, five additional perturbed spray axes were created,  
192 henceforth referred to as PD 1 – 5. For each new perturbed direction, the injection  
193 point was selected by measuring 5-mm from the centroid on the nostril plane, toward  
194 the nasopharynx. This was performed for both the left and right nostrils of Subjects  
195 1 and 2. Each new identified PD axis was evaluated using the criteria developed to  
196 identify the IU direction, and drug delivery simulations were performed following the  
197 methods described in Section 2.2. The results of the tolerance simulations were analyzed  
198 for congruity using Pearson’s correlation coefficient.

199 2.5. Experimental validation of computationally predicted spray performance

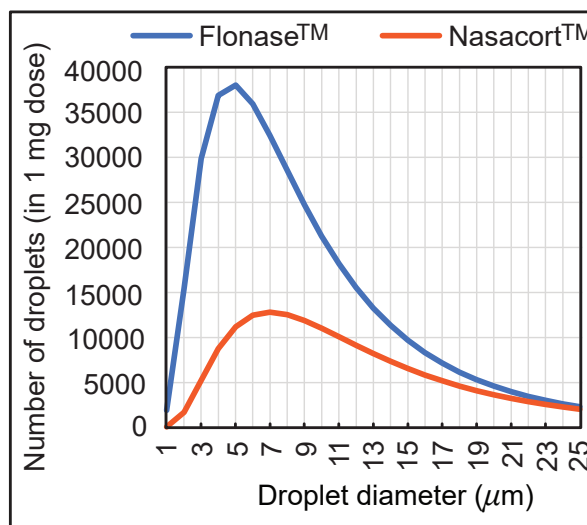
200 To extract a sense of real spray performance that could be projected from the *in*  
201 *silico* framework, we linked the computationally predicted nasopharyngeal droplet  
202 deposition efficiencies with the size distribution of droplets (see Fig. 5) in two  
203 actual over-the-counter spray products: Flonase<sup>TM</sup> (Fluticasone Propionate) and  
204 Nasacort<sup>TM</sup> (Triamcinolone Acetonide). Both are commonly prescribed medications  
205 and are commercially available. Four units of each product were tested at Next Breath,  
206 an Aptar Pharma company (Baltimore, MD, USA). The team measured the plume  
207 geometry through a SprayVIEW<sup>®</sup> NOSP, which is a non-impaction laser sheet-based  
208 instrument. With the droplet sizes in a spray shot following a log-normal distribution,  
209 the droplet size distribution (where droplet diameters are represented by  $x$ ) can be  
210 framed as a probability density function:<sup>38</sup>

$$211 \quad f(x) = \frac{1}{\sqrt{2\pi x \ln \sigma_g}} \exp \left[ -\frac{(\ln x - \ln x_{50})^2}{2(\ln \sigma_g)^2} \right]. \quad (1)$$

212 Here the mass median diameters (alternatively, the geometric mean diameter<sup>32</sup>) for  
213 Flonase<sup>TM</sup> and Nasacort<sup>TM</sup> were respectively,  $x_{50} = 37.16 \mu\text{m}$  and  $43.81 \mu\text{m}$ ; the  
214 corresponding geometric standard deviations were respectively,  $\sigma_g = 2.080$  and  $1.994$ .

215 The latter quantifies the span of the droplet size data. Note that the measurements were  
216 also collected with and without a saline additive in the sprayer, with the tests returning  
217 similar droplet size distributions. The reader is referred to our previous publications<sup>15,18</sup>  
218 for additional details.

219 To test the validity and extensibility  
220 of the computational predictions derived  
221 for real sprays, we subsequently performed  
222 multiple runs of physical spray experi-  
223 ments with 10-ml boluses (for measurable  
224 posterior deposits) of watery solutions in-  
225 jected through a 3D-printed anatomically  
226 realistic airway cavity of a different sub-  
227 ject, Subject 3 (a Caucasian male belong-  
228 ing to the age range 41-45 years; use of the  
229 subject's de-identified imaging data with  
230 CT-slice resolution of 0.352 mm was ap-  
231 proved with exempt status by the UNC  
232 Chapel Hill IRB for retrospective use).  
233 Printing of the related anterior soft plastic  
234 part on a Connex3<sup>TM</sup> 3D printer was car-  
235 ried out using polymer ink-jetting process  
236 on Tangogray FLX950 material, approxi-  
237 mately mimicking the material properties of the external nares and the internal tissues  
238 and cartilages. The 3D-printed cavity extent terminated just before the nasopharynx,  
239 thereby allowing us to measure the outflow volume of administered solution reaching  
240 nasopharyngeal walls. See the last visual under results for a pictorial representation of  
241 the 3D-printed soft nose used in the experiments.



233 **Figure 5:** Measured distribution of droplet sizes in 1-mg  
234 sprayed mass from over-the-counter Flonase<sup>TM</sup> (Fluticasone  
235 Propionate) and Nasacort<sup>TM</sup> (Triamcinolone Acetonide)  
236 spray products, over the test size range of  $\sim 1 - 24 \mu\text{m}$   
237 used for *in silico* tracking. Note that rigorous testing for  
238 droplets  $> 24 \mu\text{m}$  clearly show<sup>5</sup> that they would deposit  
239 along the anterior nasal cavity and will not directly land at  
240 the posterior target site of nasopharynx.

### 242 3. Results

#### 243 3.1. Optimal direction of spray axis and droplet sizes for effective targeting

244 Airflow and droplet tracking was simulated for spray nozzle placement in the left and  
245 right nasal airways of Subjects 1 and 2 under two standard inhalation rates (15 and 30  
246 L/min), for drug droplet diameters  $1 - 24 \mu\text{m}$ , and for the two spray directions as per  
247 the CU and IU protocols. In all eight cases, the IU direction of the spray axis results in  
248 higher deposition at the nasopharynx in comparison to the CU protocol over a defined  
249 range of particle sizes (see Fig. 6). For instance: if we examine the deposition trends  
250 for spray administration through the right nostril of Subject 2 for the laminar regime  
251 inhalation (i.e. at 15 L/min), the peak nasopharyngeal deposition for IU is 46.5% for  
252  $13 \mu\text{m}$  drug droplets (Fig. 6(b)), while the peak deposition for CU is only 0.53% for  
253  $14 \mu\text{m}$  drug droplets (see again Fig. 6(b) and the corresponding zoomed-in for the CU



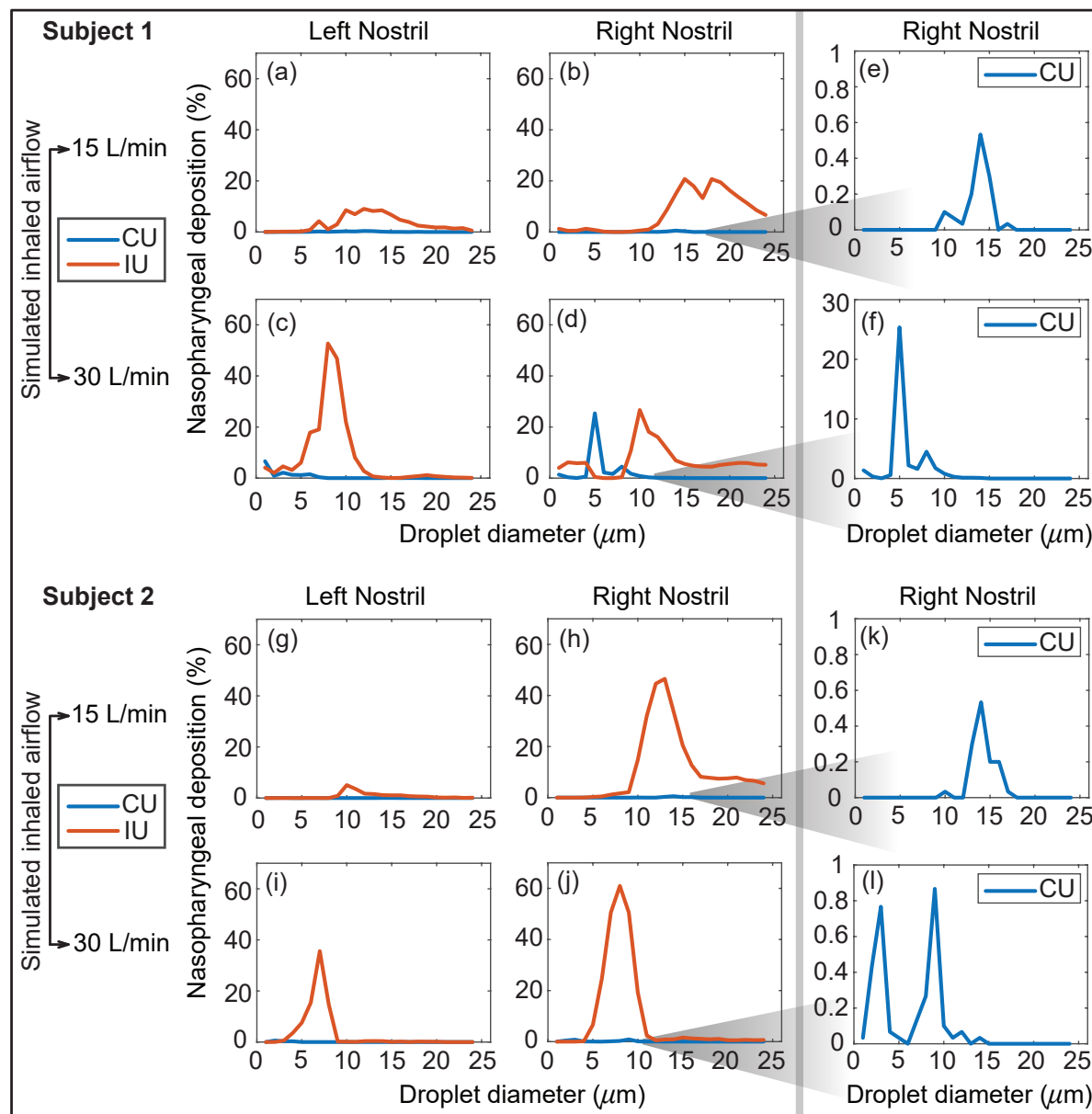


**Figure 6:** Panels (a) – (d) show the comparison of the regional deposition trends at the nasopharynx of Subject 1, for the IU and CU protocols, with monodispersed conical injections. The rows (a) – (b) are for 15 L/min inhalation; rows (c) – (d) are for 30 L/min inhalation. Panels (e) – (f) depict the representative zoomed-in trends for nasopharyngeal deposition with the CU protocol, on administering the spray through the right nostril. Similarly, panels (g) – (j) show the comparison of the regional deposition trends at the nasopharynx of Subject 2, for the IU and CU protocols. The rows (g) – (h) are for 15 L/min inhalation; rows (i) – (j) are for 30 L/min inhalation. Panels (k) – (l) depict the representative zoomed-in trends for nasopharyngeal deposition with the CU protocol, on administering the spray through the right nostril. The IU trend lines are marked in red; the CU trend lines are in blue. The reader should note the abbreviated vertical range on the (e) – (f) and (k) – (l) plots, prompted by the 2 orders-of-magnitude smaller deposition efficiency with CU.

254 delivery trends visual in Fig. 6(k)). In general, the droplet size range of  $\sim 6 - 14 \mu\text{m}$  is  
 255 found conducive to targeted nasopharyngeal delivery with the IU protocol, considering  
 256 a 2% cut-off for deposition efficiency of the tracked monodispersed droplet cluster of  
 257 each size. The nearly hundred-fold increase in targeted deposition is remarkable and is  
 258 achievable simply by re-orienting the spray axis from CU to IU.

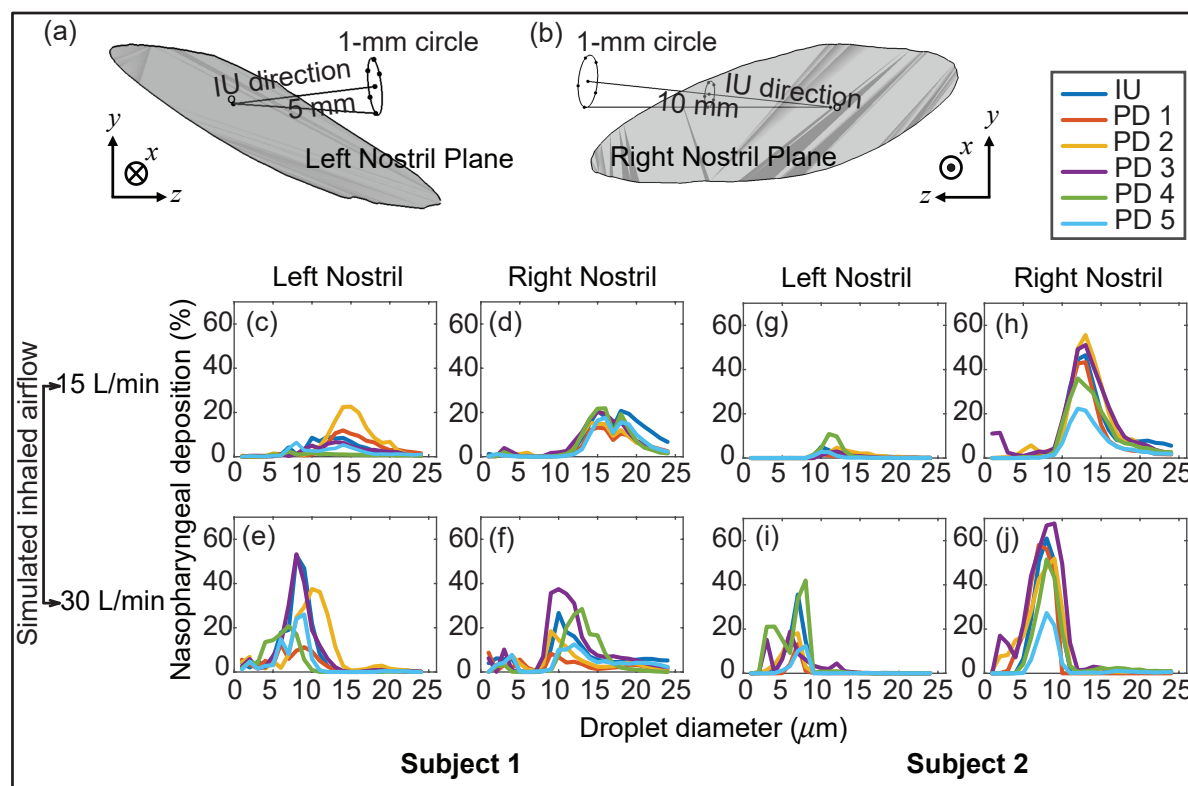


**Figure 7:** Panels (a) and (b) illustrate the *in silico* detection of the perturbed spray directions (PD), deviating slightly from the IU axis. The direction vectors are from the centroid of the nostril plane to the points lying on a 1-mm circle that is 5 mm and 10 mm (respectively for the left and right nostril placement) from the nostril plane centroid (see Section 2.4 for associated details). Panels (c) – (f) for Subject 1 and panels (g) – (j) for Subject 2 compare the respective nasopharyngeal deposition trends for PD 1 – 5 directions, with respect to that of the “Improved Use” (IU) protocol. The top row is for 15 L/min inhalation; the bottom row is for 30 L/min inhalation rate. Clustering of the plots signifies robustness of the IU usage parameters; in other words, the IU protocol is satisfactorily less sensitive to user subjectivities.

### 259 3.2. Assessing sensitivity to IU perturbations

260 The variation of the nasopharyngeal deposition percentages over the assessed droplet size  
 261 range (1 – 24 μm) was compared between that of the IU protocol and for each of the PD  
 262 1 – 5 cases. Pearson’s correlation coefficient was greater than 0.5 for nearly every such  
 263 comparison (see Fig. 7 and Table 1), showing a high degree of linearity between the new  
 264 perturbed directions and the IU protocol. Moreover, the p-value associated with each  
 265 correlation was much lower than the significance level, i.e. 0.05. This indicates that there  
 266 is a statistically significant correlation between the simulation results on the targeted  
 267 nasopharyngeal drug delivery for the IU and the perturbed directions. Physically, the  
 268 satisfactory correlation between IU and PD 1 – 5 establishes the robustness of the IU  
 269 spray protocol to user subjectivities.

### 270 3.3. Verification of optimal droplet sizes through scaling analysis

271 The droplet size ranges that registered peak nasopharyngeal deposition under each  
 272 inhalation condition were further analyzed and validated for reliability, through a Stokes

273 number-based scaling analysis.<sup>39</sup> The Stokes number (St) is defined as<sup>32</sup>

$$274 \quad \text{St} = \frac{U \rho_{\mathbb{D}} \mathbb{D}^2 C_c}{18 \mu d}, \quad (2)$$

275 where  $U$  for the present system is the airflow rate divided by flux area,  $\rho_{\mathbb{D}}$  is the material  
276 density of the inhaled droplets,  $C_c$  is the Cunningham slip correction factor,  $\mu$  is the  
277 dynamic viscosity of the ambient medium i.e. air, and  $d$  represents the characteristic  
278 diameter of the flux cross-section. Now, all other flow and morphological parameters  
279 staying invariant, Equation 2 directly leads to the following scaling law:

$$280 \quad \frac{\mathbb{D}_2}{\mathbb{D}_1} = \sqrt{\frac{Q_1}{Q_2}}. \quad (3)$$

281 Herein  $(Q_i, \mathbb{D}_i)$  are different airflow rate and droplet size pairings. Let us now consider  
282 a representative example, say the right nostril spray administration in Subject 2. For  
283 at least 2% nasopharyngeal deposition, the computationally predicted ideal droplet size  
284 range during 30 L/min inhalation is  $[\mathbb{D}_{\min}, \mathbb{D}_{\max}] = [5, 11] \mu\text{m}$ . Equation 3 can  
285 consequently help us to project the corresponding ideal size range at the lower inhalation  
286 rate of 15 L/min. If the to-be-projected droplet size range that would generate peak  
287 nasopharyngeal deposition during the latter case is represented by  $[\mathbb{D}'_{\min}, \mathbb{D}'_{\max}]$  in  $\mu\text{m}$ ,  
288 then

$$289 \quad \frac{\mathbb{D}'_{\min}}{5} = \frac{\mathbb{D}'_{\max}}{11} = \sqrt{\frac{30}{15}}. \quad (4)$$

290 This results in  $\mathbb{D}'_{\min} = 7.07 \mu$  and  $\mathbb{D}'_{\max} = 15.56 \mu$ . Despite the simplicity of this  
291 scaling analysis, the computationally identified range 9 – 24  $\mu\text{m}$  for the same breathing  
292 conditions hence follows the same trend on the number scale, in terms of the respective  
293 variations from the extremal limits of  $[\mathbb{D}_{\min}, \mathbb{D}_{\max}]$ . The penultimate panel in Fig. 8  
294 visually illustrates this specific example; see the remaining panels in Fig. 8 for all the  
295 other test cases. The directional change of the extremal limits for the St-projected ideal  
296 droplet size ranges remarkably agrees with the corresponding CFD-based size ranges in  
297 all cases, except in one trivial outlier: see panel (c) for Subject 1's right nostril, there  
298 the maximum ideal size limits for both 15 and 30 L/min are 24  $\mu\text{m}$ ; the St-projected  
299 maximum ideal droplet size for 30 L/min is, however, 33.94  $\mu\text{m}$ .

### 300 3.4. Comparison of the *in silico* findings to physical experiments

301 Panel (a) in Fig. 9 portrays the order-of-magnitude improvement in targeted drug  
302 deposition at the nasopharynx (with the IU protocol over the CU protocol), when  
303 taking into the account the droplet size distributions<sup>15,18</sup> in real over-the-counter spray  
304 products, *viz.* Flonase<sup>TM</sup> and Nasacort<sup>TM</sup>, in an administered shot. See Section 2.5  
305 for the related study methods. Considering all the test cases, the average IU-over-CU  
306 improvement for the two chosen spray products, as projected from the CFD simulations,  
307 was 2.117 orders-of-magnitude with a standard deviation of 0.506 orders. The physical  
308 experiments in Subject 3 (presenting an entirely different anatomy) show a comparable

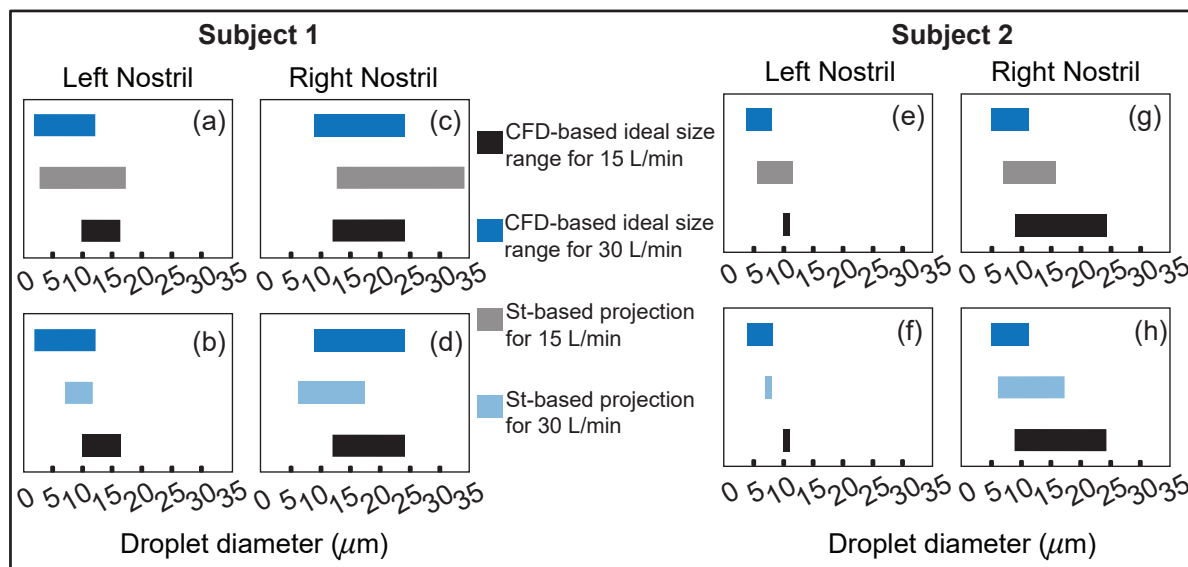


**Figure 8:** Panels (a) – (d) for Subject 1 and panels (e) – (h) for Subject 2 visually depict the Stokes number (St)-based projections of ideal droplet size ranges for maximal targeted deposition at the nasopharynx. The directional change of the St-projected ranges agree with the corresponding CFD-based ideal droplet size ranges in all the test cases, except in one trivial outlier: see panel (c), where the maximum ideal size limits for both 15 and 30 L/min are 24  $\mu\text{m}$ ; the St-projected maximum ideal droplet size for 30 L/min is, however, 33.94  $\mu\text{m}$ . See Section 3.3 for a representative discussion for the data reported in (g).

309 improvement in nasopharyngeal delivery, by 2.215 orders-of-magnitude, with a standard  
 310 deviation of 0.016 orders. Panel (b) in Fig. 9 plots the experimental measurements.  
 311 Hence, the computational predictions differ from the *in vitro* data by less than 5%,  
 312 thereby lending robust support to the implemented *in silico* framework.

#### 313 4. Discussion

- 314 • *On inputs to targeted drug design* – With targeted delivery of pharmaceutical agents to  
 315 the viral infection hot-spots in the posterior upper airway (e.g. at the nasopharynx)

**Table 1:** Statistical testing on the correlation between the regional deposition trends (for different drug droplet sizes) at the nasopharynx for the perturbed spray directions (i.e. PD 1 – 5), when compared to the nasopharyngeal deposition with the IU protocol.

Model	Simulation Case	Pearson's Correlation Coefficient (r)					p-value associated with correlation				
		PD 1	PD 2	PD 3	PD 4	PD 5	PD 1	PD 2	PD 3	PD 4	PD 5
Subject 1	Left Nostril Administration 15 L/min Inhalation	0.6805	0.6745	0.9176	0.6155	0.6620	2.53E-04	3.01E-04	2.78E-10	1.37E-03	4.26E-04
	Right Nostril Administration 15 L/min Inhalation	0.9526	0.8795	0.8469	0.8769	0.9580	7.43E-13	1.52E-08	1.80E-07	1.89E-08	2.01E-13
	Left Nostril Administration 30 L/min Inhalation	0.8191	0.6122	0.9725	0.5525	0.9577	9.87E-07	1.48E-03	2.07E-15	5.12E-03	2.22E-13
	Right Nostril Administration 30 L/min Inhalation	0.4607	0.7348	0.8711	0.5499	0.8029	2.35E-02	4.33E-05	3.06E-08	5.37E-03	2.34E-06
Subject 2	Left Nostril Administration 15 L/min Inhalation	0.9548	0.6513	0.7114	0.7296	0.9343	4.49E-13	5.66E-04	9.72E-05	5.21E-05	2.49E-11
	Right Nostril Administration 15 L/min Inhalation	0.9848	0.9629	0.9523	0.9805	0.9939	3.24E-18	5.29E-14	8.03E-13	4.77E-17	1.50E-22
	Left Nostril Administration 30 L/min Inhalation	0.9348	0.8904	0.5591	0.7557	0.8534	2.29E-11	5.66E-09	4.51E-03	1.95E-05	1.16E-07
	Right Nostril Administration 30 L/min Inhalation	0.9413	0.9512	0.9387	0.9877	0.9797	7.53E-12	1.02E-12	1.18E-11	3.05E-19	7.44E-17



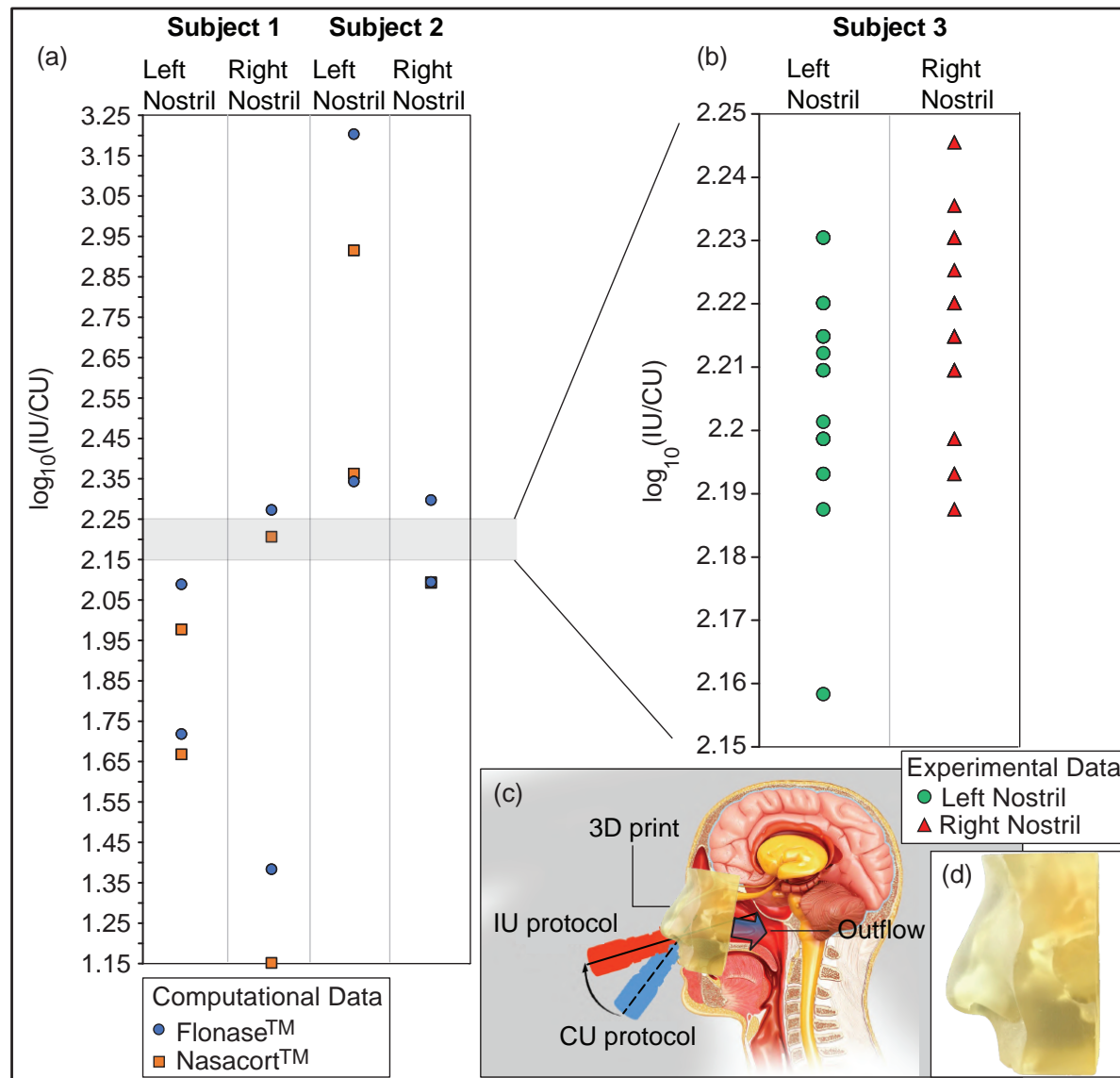


**Figure 9:** Panel (a) shows the order-of-magnitude IU-induced improvement in drug mass deposits at the nasopharynx of Subjects 1 and 2 (when compared to the CU delivery numbers), while considering the droplet size distribution in each administered shot of two common over-the-counter spray products: Flonase™ and Nasacort™. Panel (b) shows the measurements from a set of physical experiments with sprayed watery solution in different Subject 3. As an indicator for agreement between the computational and experimental projections, the vertical range in (b) is a medial subset of that in (a). Note that several data-points roughly superimposed over each other, in both (a) and (b). Panel (c) presents a cartoon of the experimental setup. A separate in-set visual for the 3D-printed soft nose, with realistically pliable external nares, is shown in (d).

316 a clear challenge,<sup>15,40,41</sup> the experimentally-validated findings (see Fig. 6) from this  
 317 study point to the droplet size range of  $\sim 6 - 14 \mu\text{m}$  as being the most effective  
 318 at maximizing the sprayed and inhaled percentage deposition at the clinical upper  
 319 airway target site for SARS-like infections. The information could be utilized to  
 320 design next-generation intranasal drug formulations, along with novel spray devices  
 321 and atomizers.

- 322 • *On inputs for effective spray usage strategies* – The significant 2 orders-of-magnitude  
 323 improvement (see Fig. 9) in nasopharyngeal delivery of intranasally sprayed drugs with

324 the new IU protocol, over the typically recommended CU protocol, clearly warrants a  
325 revisit of the standard usage instructions for existing nasal spray products. While  
326 Section 2.3 lays out the different criteria points for *in silico* detection of the IU  
327 direction†; in ordinary language: the user can replicate the IU protocol by holding  
328 spray nozzle as horizontally as possible at the nostril, with a slight tilt towards the  
329 cheeks and pointed a little at the outer edge of the eye (e.g., right eye if one is placing  
330 the spray at the right nostril). See Fig. 10 for a sample demonstration.

331 • *On the limitations of respiratory flow modeling* – The reader should note that a  
332 realistic modeling of mucociliary transport along the morphologically complex airway  
333 cavity constitutes a significant open question in the domains respiratory transport  
334 mechanics.<sup>42</sup> In this study, we have implemented state-of-the-art algorithms to  
335 identify the droplet sizes that are efficient at *direct* nasopharyngeal delivery, under  
336 the impact of inhaled airflow when sprayed into the intranasal space. However, a big  
337 caveat lies in what happens to the larger droplets that happen to deposit along the  
338 anterior parts of the airway. Quantifying their mucus-driven downstream transport  
339 mechanics and correlating that with the therapeutic efficacy of the drug solutes when  
340 they reach the posterior clinical target sites poses a major translational challenge, to  
341 be addressed by the community in future.

342 • *On the constraints posed by the reconstructed in silico geometries* – The CT-based  
343 anatomically realistic reconstructions, while accurately replicating the topological  
344 convolutions implicit in a real tortuous respiratory cavity, still come with the caveat  
345 of containing structurally rigid airway walls. However, though the rigidity of the walls  
346 (intended to mimic the internal tissue surfaces and cartilages) is somewhat unrealistic,  
347 the time-scale of inhaled transport is on the scale of  $10^{-1}$  s.<sup>18</sup> and the idealization  
348 could be considered a mechanically feasible assumption that is sufficient to extract the  
349 fundamental nuances underlying such physiologically complex transport processes.

350 • *On the usability of the findings despite the small test cohort* – Clearly the current study  
351 is somewhat limited given the restricted sample size of only two main test subjects  
352 (i.e. Subjects 1 and 2). However, the congruity in targeted delivery improvement  
353 (see Section 3.4 and Fig. 9) in a randomly-selected third subject (Subject 3) bodes  
354 well for the general extensibility of the essential findings to a wider cohort. At the  
355 least, the results presented here, though preliminary in essence given the small cohort  
356 size, could be considered an important step in the mechanistic characterization of  
357 the respiratory transmission dynamics for improving the performance of intranasally  
358 administered spray products.

359 • *On toxicity evaluation* – Any new formulation or drug delivery device that might  
360 attempt to replicate the improved targeted deposition at intranasal sites, based on  
361 the current findings, will essentially form a surface contacting mechanism with limited

† (i) Extended spray axis for the IU protocol intersects the nasopharynx; (ii) as a condition for clinical safety (based on recommendation from attending rhinologists<sup>15,37</sup>), the axis must not cut through the septum; (iii) the spray axis should intersect the lateral wall of the nasal cavity as posteriorly as feasible.

362 duration contact. For determination of usage safety levels, such a development will  
363 also require biocompatibility testing of the device, including check of three basic  
364 biocompatibility endpoints (i.e., cytotoxicity, irritation,<sup>43</sup> sensitization) per the Food  
365 and Drug Administration (FDA) guidance,<sup>44,45</sup> by providing test data and/or relevant  
366 justification (e.g., history of clinical use for the same device).

## 367 5. Final takeaways

368 Intranasal sprays could represent a useful ad-  
369 ministration strategy for nasal hygiene products,  
370 prophylactics, and antivirals – for respiratory  
371 pathogens that would first trigger an upper air-  
372 way infection, such as SARS-CoV-2. In this study,  
373 we have used computational fluid dynamics simu-  
374 lations to illustrate that simple tweaks to the nasal  
375 spray direction can result in vastly improved drug  
376 delivery to the critical viral infection sites inside  
377 the nose, more specifically the delivered dose reg-  
378 isters an approximately 2 orders-of-magnitude im-  
379 provement. The proposed IU protocol (see Figs. 3  
380 and 4; also Fig. 10) is easy-to-replicate and has  
381 been verified to be robust to small perturbations  
382 that may stem from user subjectivities. Also, the droplet size range of  $\sim 6 - 14 \mu\text{m}$   
383 is found most efficient at facilitating direct delivery of intranasally sprayed drug par-  
384 ticulates at the nasopharynx, which is the dominant infection trigger zone. Both these  
385 key pieces of findings bear the promise for developing increasingly effective intranasal  
386 pharmaceutical formulations, along with upgraded designs for nasal drug delivery devices  
387 and atomizers.

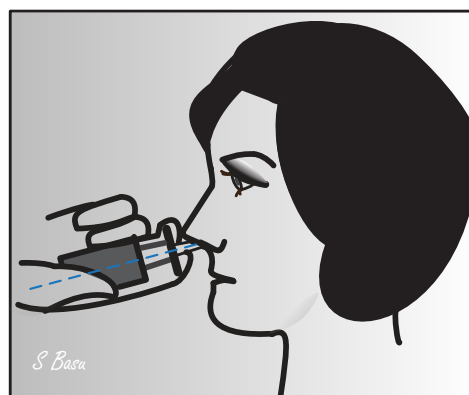


**Figure 10:** Demonstrative sagittal sketch for the “Improved Use” (IU) protocol, outlining how to hold a spray bottle during intranasal administration. Illustration is by the lead author.

388

## 389 Acknowledgements

390 The authors thank the *Bioinspiration & Biomimetics* editorial board for the invitation  
391 to publish. This material is based on work partially supported by the National Science  
392 Foundation (NSF) RAPID Grant 2028069 for COVID-19 research, with SB as the Co-  
393 Principal Investigator. Any opinions, findings, and conclusions or recommendations  
394 expressed here are, however, those of the authors and do not necessarily reflect views of  
395 the NSF.

396 **Author contributions**

397 SB, DJM, AC conceived this study; SB developed the study protocol, the anatomic  
398 reconstructions and drafted the manuscript; MMHA carried out the physical  
399 experiments and the theoretical analysis; SB, YL, PAB, PA, NKK performed the  
400 numerical simulations; AM, ZS processed the computational data; JS tested the over-  
401 the-counter spray products; SB and DJM jointly supervised the student researchers  
402 (MMHA, YL, PAB, PA, NKK, AM, ZS).

403 **Conflicts of interest**

404 The authors declare no competing interests.

405

---

406 **References**

407

- 408 [1] Johns-Hopkins-University. Coronavirus Resource Center. Web link, accessed 15-January-2022.  
409 [2] R. Mittal, R. Ni, and J. H. Seo. The flow physics of COVID-19. *Journal of Fluid Mechanics*, 894,  
410 2020.  
411 [3] Y. J. Hou, K. Okuda, C. E. Edwards, D. R. Martinez, T. Asakura, K. H. Dinnon III, T. Kato,  
412 R. E. Lee, B. L. Yount, T. M. Mascenik, et al. SARS-CoV-2 Reverse Genetics Reveals a Variable  
413 Infection Gradient in the Respiratory Tract. *Cell*, 2020.  
414 [4] N. J. Matheson and P. J. Lehner. How does SARS-CoV-2 cause COVID-19? *Science*,  
415 369(6503):510–511, 2020.  
416 [5] S. Basu. Computational characterization of inhaled droplet transport to the nasopharynx.  
417 *Scientific Reports*, 11:1–13, 2021.  
418 [6] X. He, E. H. Y. Lau, P. Wu, X. Deng, J. Wang, X. Hao, Y. C. Lau, J. Y. Wong, Y. Guan, X. Tan,  
419 et al. Temporal dynamics in viral shedding and transmissibility of COVID-19. *Nature Medicine*,  
420 26(5):672–675, 2020.  
421 [7] W. Sungnak, N. Huang, C. Bécaivin, M. Berg, R. Queen, M. Litvinukova, C. Talavera-López,  
422 H. Maatz, D. Reichart, F. Sampaziotis, et al. SARS-CoV-2 entry factors are highly expressed  
423 in nasal epithelial cells together with innate immune genes. *Nature Medicine*, 26(5):681–687,  
424 2020.  
425 [8] S. Basu, N. S. Hochberg, B. A. Senior, D. Joseph-McCarthy, and A. Chakravarty. From SARS-  
426 CoV-2 infection to COVID-19 disease: a proposed mechanism for viral spread to the lower  
427 airway based on in silico estimation of virion flow rates. *medRxiv*, 2020.  
428 [9] S. Basu, M. M. H. Akash, N. S. Hochberg, B. A. Senior, D. Joseph-McCarthy, and A. Chakravarty.  
429 From SARS-CoV-2 infection to COVID-19 morbidity: an in silico projection of virion flow rates  
430 to the lower airway via nasopharyngeal fluid boluses. *Rhinology Online*, 2022.  
431 [10] M. Pachetti, B. Marini, F. Benedetti, F. Giudici, E. Mauro, P. Storici, C. Masciovecchio,  
432 S. Angeletti, M. Ciccozzi, R. C. Gallo, et al. Emerging SARS-CoV-2 mutation hot spots include  
433 a novel RNA-dependent-RNA polymerase variant. *Journal of Translational Medicine*, 18(1):1–9,  
434 2020.  
435 [11] G. J. M. Garcia, J. D. Schroeter, R. A. Segal, J. Stanek, G. L. Foureman, and J. S. Kimbell.  
436 Dosimetry of nasal uptake of water-soluble and reactive gases: a first study of interhuman  
437 variability. *Inhalation Toxicology*, 21(7):607–618, 2009.  
438 [12] M. M. H. Akash, A. Mituniewicz, Y. Lao, P. Balivada, P. Ato, N. Ka, Z. Silfen, A. Chakravarty,



- 439 D. Joseph-McCarthy, and S. Basu. A better way to spray?—a model-based optimization of nasal  
440 spray use protocols. *Bulletin of the American Physical Society*, 2021.
- 441 [13] D. O. Frank-Ito, M. Wofford, J. D. Schroeter, and J. S. Kimbell. Influence of mesh density on  
442 airflow and particle deposition in sinonasal airway modeling. *Journal of Aerosol Medicine and*  
443 *Pulmonary Drug Delivery*, 29(1):46–56, 2016.
- 444 [14] S. Basu, N. Witten, and J. S. Kimbell. Influence of localized mesh refinement on numerical  
445 simulations of post-surgical sinonasal airflow. *Journal of Aerosol Medicine and Pulmonary Drug*  
446 *Delivery*, 30(3):A–14, 2017.
- 447 [15] S. Basu, L. T. Holbrook, K. Kudlaty, O. Fasanmade, J. Wu, A. Burke, B. W. Langworthy, Z. Farzal,  
448 M. Mamdani, W. D. Bennett, J. P. Fine, B. A. Senior, et al. Numerical evaluation of spray  
449 position for improved nasal drug delivery. *Scientific Reports*, 10(1):1–18, 2020.
- 450 [16] K. Inthavong, J. Ma, Y. Shang, J. Dong, A. S. R. Chetty, J. Tu, and D. O. Frank-Ito. Geometry  
451 and airflow dynamics analysis in the nasal cavity during inhalation. *Clinical Biomechanics*,  
452 66:97–106, 2019.
- 453 [17] Y. Zhang, Y. Shang, K. Inthavong, Z. Tong, B. Sun, K. Zhu, A. Yu, and G. Zheng. Computational  
454 investigation of dust mite allergens in a realistic human nasal cavity. *Inhalation Toxicology*,  
455 31(6):224–235, 2019.
- 456 [18] S. Basu, D. O. Frank-Ito, and J. S. Kimbell. On computational fluid dynamics models for sinonasal  
457 drug transport: Relevance of nozzle subtraction and nasal vestibular dilation. *International*  
458 *Journal for Numerical Methods in Biomedical Engineering*, 34(4):e2946, 2018.
- 459 [19] Z. Farzal, S. Basu, A. Burke, O. O. Fasanmade, E. M. Lopez, W. D. Bennett, C. S. Ebert Jr,  
460 A. M. Zanation, B. A. Senior, and J. S. Kimbell. Comparative study of simulated nebulized and  
461 spray particle deposition in chronic rhinosinusitis patients. In *International Forum of Allergy*  
462 *& Rhinology*, volume 9, pages 746–758. Wiley Online Library, 2019.
- 463 [20] J. S. Kimbell, S. Basu, G. J. M. Garcia, D. O. Frank-Ito, F. Lazarow, E. Su, D. Protsenko, Z. Chen,  
464 J. S. Rhee, and B. J. Wong. Upper airway reconstruction using long-range optical coherence  
465 tomography: Effects of airway curvature on airflow resistance. *Lasers in Surgery and Medicine*,  
466 51(2):150–160, 2019.
- 467 [21] S. Basu and M. A. Stremler. Exploring the dynamics of ‘2P’ wakes with reflective symmetry using  
468 point vortices. *Journal of Fluid Mechanics*, 831:72–100, 2017.
- 469 [22] S. Basu and M. A. Stremler. On the motion of two point vortex pairs with glide-reflective symmetry  
470 in a periodic strip. *Physics of Fluids*, 27(10):103603, 2015.
- 471 [23] M. A. Stremler and S. Basu. On point vortex models of exotic bluff body wakes. *Fluid Dynamics*  
472 *Research*, 46(6):061410, 2014.
- 473 [24] P. W. Longest and S. Vinchurkar. Validating CFD predictions of respiratory aerosol deposition:  
474 effects of upstream transition and turbulence. *Journal of biomechanics*, 40(2):305–316, 2007.
- 475 [25] E. L. Perkins, S. Basu, G. J. M. Garcia, R. A. Buckmire, R. N. Shah, and J. S. Kimbell.  
476 Ideal particle sizes for inhaled steroids targeting vocal granulomas: preliminary study using  
477 computational fluid dynamics. *Otolaryngology–Head and Neck Surgery*, 158(3):511–519, 2018.
- 478 [26] S. Hosseini, T. A. Schuman, R. Walenga, J. V. Wilkins Jr, A. Babiskin, and L. Golshahi. Use of  
479 anatomically-accurate 3-dimensional nasal airway models of adult human subjects in a novel  
480 methodology to identify and evaluate the internal nasal valve. *Computers in Biology and*  
481 *Medicine*, page 103896, 2020.
- 482 [27] D. J. Doorly, D. J. Taylor, and R. C. Schroter. Mechanics of airflow in the human nasal airways.  
483 *Respiratory Physiology & Neurobiology*, 163(1-3):100–110, 2008.
- 484 [28] N. Baghernezhad and O. Abouali. Different SGS models in Large Eddy Simulation of 90 degree  
485 square cross-section bends. *Journal of Turbulence*, (11):N50, 2010.
- 486 [29] Aptar Pharma. Valos VP7 Spray Pump. White Paper link, accessed 18-January-2022.
- 487 [30] X. Liu, W. H. Doub, and C. Guo. Assessment of the influence factors on nasal spray droplet  
488 velocity using phase-Doppler anemometry. *AAPS Pharmscitech*, 12(1):337–343, 2011.
- 489 [31] S. Basu, Z. Farzal, and J. S. Kimbell. “Magical” fluid pathways: inspired airflow corridors for

- 490 optimal drug delivery to human sinuses. In *APS Division of Fluid Dynamics Meeting Abstracts*,  
491 pages L4-004, 2017.
- 492 [32] W. H. Finlay. *The Mechanics of Inhaled Pharmaceutical Aerosols: An Introduction*. Academic  
493 Press, 2001.
- 494 [33] M. S. Benninger, J. A. Hadley, J. D. Osguthorpe, B. F. Marple, D. A. Leopold, M. J. Derebery,  
495 and M. Hannley. Techniques of intranasal steroid use. *Otolaryngology – Head and Neck Surgery*,  
496 130(1):5–24, 2004.
- 497 [34] V. Kundoor and R. N. Dalby. Effect of formulation-and administration-related variables on  
498 deposition pattern of nasal spray pumps evaluated using a nasal cast. *Pharmaceutical Research*,  
499 28(8):1895–1904, 2011.
- 500 [35] Fluticasone propionate nasal spray instructions. [http://dailymed.nlm.nih.gov/dailymed/  
501 archives/fdaDrugInfo.cfm?archiveid=5767](http://dailymed.nlm.nih.gov/dailymed/archives/fdaDrugInfo.cfm?archiveid=5767). accessed 21-September-2013.
- 502 [36] J. S. Kimbell, S. Basu, Z. Farzal, and B. A. Senior. Characterizing nasal delivery in 3D models  
503 before and after sinus surgery. *Respiratory Drug Delivery*, 1:181–188, 2018.
- 504 [37] S. Treat, C. S. Ebert Jr, Z. Farzal, S. Basu, A. M. Zanation, B. D. Thorp, J. S. Kimbell, B. A.  
505 Senior, and A. J. Kimple. Intranasal corticosteroids: patient administration angles and impact  
506 of education. *Rhinology Online*, 2020.
- 507 [38] Y. S. Cheng, T. D. Holmes, J. Gao, R. A. Guilmette, S. Li, Y. Surakitbanharn, and C. Rowlings.  
508 Characterization of nasal spray pumps and deposition pattern in a replica of the human nasal  
509 airway. *Journal of Aerosol Medicine*, 14(2):267–280, 2001.
- 510 [39] S. Balachandar. A scaling analysis for point-particle approaches to turbulent multiphase flows.  
511 *International Journal of Multiphase Flow*, 35(9):801–810, 2009.
- 512 [40] J. Suman. How evolving patient needs have fuelled the development of nasal drug delivery, 2021.
- 513 [41] S. A. Shah, C. J. Dickens, D. J. Ward, A. A. Banaszek, C. George, and W. Horodnik. Design of  
514 experiments to optimize an in vitro cast to predict human nasal drug deposition. *Journal of  
515 Aerosol Medicine and Pulmonary Drug Delivery*, 27(1):21–29, 2014.
- 516 [42] A. G. Ford, X. Z. Cao, M. J. Papanikolas, T. Kato, R. C. Boucher, M. R. Markovetz, D. B.  
517 Hill, R. Freeman, and M. G. Forest. Molecular dynamics simulations to explore the structure  
518 and rheological properties of normal and hyperconcentrated airway mucus. *Studies in Applied  
519 Mathematics*, 2021.
- 520 [43] S. Basu, U. A. Khawaja, S. A. A. Rizvi, B. Gong, W. Yeung, M. A. Sanchez-Gonzalez, and  
521 G. Ferrer. Evaluation of patient experience for a computationally-guided intranasal spray  
522 protocol to augment therapeutic penetration. *medRxiv*, 2021.
- 523 [44] ISO. Biological evaluation of medical devices – Part 1: Evaluation and testing within a risk  
524 management process. *ISO 10993-1: 2009*, 2009.
- 525 [45] Use of International Standard ISO 10993-1, “Biological evaluation of medical devices – Part 1:  
526 Evaluation and testing within a risk management proces” – Guidance for Industry and Food  
527 and Drug Administration Staff. <https://www.fda.gov/media/85865/download>. accessed 23-  
528 January-2022.